A NOVEL MODULAR ARCHITECTURE FOR A NEURAL CONTROLLER FOR PREDICTIVE SIMULATIONS OF STAND-TO-WALK MOTIONS

A PREPRINT

David Muñoz*
School of Electrical and Electronic Engineering
University College Dublin
Dublin, Ireland
david.munoz@ucdconnect.ie

Donal Holland
School of Mechanical and Materials Engineering
University College Dublin
Dublin, Ireland
donal.holland@ucd.ie

Giacomo Severini
School of Electrical and Electronic Engineering
University College Dublin
Dublin, Ireland
giacomo.severini@ucd.ie

December 13, 2023

ABSTRACT

Predictive neuromuscular models are a powerful tool for testing assumptions on the underlying architecture of sensorimotor control and its associated neural activity. These models can test hypotheses that conventional methods of assessment cannot evaluate directly. However, current models are generally task-specific and mapping completely the skill space of a motion requires the tuning of all the parameters of the system. We here propose a modular model for Posture and Locomotion (MPL model), where a hierarchical architecture organizes modules in specific activation networks to accomplish motion tasks. A higher control layer, represented by a hypothetical mesencephalic locomotor region (MLR), sends controlling signals that manage motions and maps the skill space. The switch of motions is reflected by the activation of internal models (IMs). The IMs organize modules called synergies, that are coactivated sensory responses mapping multiple muscles, to display different motor behaviours. This architecture was tested in stand-to-walk (STW) simulations, where two IMs recombine five synergies to replicate 'stand' and 'walk'. The model was successful in replicating a STW transition in a single simulation. The kinematics, muscle activation patterns and ground reaction forces during walking are consistent with experimental data. The model is also able to transition to slower and faster speeds by tuning the controlling signal once steady gait is reached. The proposed architecture is expected to be a first step to create neuromuscular models which integrate multiple motor behaviours in a unified controller.

Keywords Predictive neuromuscular simulations · Stand-To-Walk · Synergies · Modular controller · Speed transitions

1 Introduction

Predictive Neuromuscular Modelling (PNM) can address the gaps in the knowledge of human locomotion by testing hypotheses about the inherent neurophysiology of gait [De Groote and Falisse, 2021]. PNM can be used to devise the commands relative to a task, characterized by an objective function, at the level of the actuators [De Groote et al.,

*Use footnote for providing further information about author (webpage, alternative address)—*not* for acknowledging funding agencies.

2016, Falisse et al., 2019] or of a hypothetical control architecture [Di Russo et al., 2023, Taga et al., 1991, Geyer and Herr, 2010, Muñoz et al., 2022]. In the latter case, the hypothetical motor control is implemented as a control policy, consisting of a set of equations representing ruling principles of motion. The control policy reflects inputs, transformations, and outputs of the system. The inputs define the prime commands of the system that can be generated by higher structures. These inputs map to feedforward and feedback control schemes. The transformations convert the inputs to the expected motor responses and should represent specific aspects of human neurophysiology. The output is a set of last-level commands that, when applied to a substrate such as a musculoskeletal model, can generate motions that mimic one or more elements of the human locomotion skill space. Motor control hypotheses can then be tested through models by comparing the output of the simulations with data collected in experimental conditions.

Current controller-based neuromuscular models have been partially successful in replicating human gait or representing it according to neurophysiological principles. CPG-based (Central Pattern Generators) models regulate gait speed and walk-to-run transitions applying a unidimensional control [Taga et al., 1991]. Reflex-based models implement reflexes which are well documented in neurophysiological experiments [Geyer and Herr, 2010] and have been shown to replicate well steady-state gait behaviors. However, evidence suggests that CPG, if they exist in humans, would be dependent on an intact sensory system to generate locomotion [Capaday, 2002]. Hybrid models encompassing both reflexes, CPGs, or other components of feedforward control [Di Russo et al., 2023, Ramadan et al., 2021] show versatility and physiological plausibility, and appear to better capture the complexity of human locomotor control. However, controller-based PNM to this day has presented only control architectures that are specific to a task (usually steady state gait) and do not present the flexibility for representing drastically different gait and balance behaviors.

Here we propose a novel hybrid modular architecture that builds upon current literature on hybrid CPG/reflex models and neurophysiology and can replicate different behaviors. The motor control hypothesis we here implemented consists of higher layers in the CNS, corresponding to simplifications the Internal Models [Wolpert et al., 1998, Kawato, 1999], rearranging motor responses in the spinal cord to accomplish specific motor tasks. The hypothesis we present is based on four assumptions: i) motion can be mapped to a correct arrangement of modular elements located in the spinal cord [Caggiano et al., 2016]; ii) some of these elements have a reflexive nature and stimulate more than one muscle in synergy [Ivanenko et al., 2006]; iii) a neural pathway is the result of applying a specific pattern of excitatory and inhibitory synapses, here referred to as an internal model (IM), to a set of synergies [Levine et al., 2014]; iv) a hypothetical higher layer, corresponding to the mesencephalic locomotor region (MLR), selects IMs in parallel or sequentially to accomplish specific objectives [Le Ray et al., 2011].

This system, called the Modular Posture and Locomotion model (MPL model), is applied to a stand-to-walk (STW) simulation. Five synergies are used to replicate 'stand' and 'walking', and one more to ease the transition between them. The synergies are designed as independent reflex loops. However, when they are combined by the internal models, stereotyped motor responses emerge to display 'stand' or 'gait'.

Synergies represent principles of legged mechanics (Fig. 1) and are proposed as an alternative to the traditional concept of human CPG. In this model, the rhythmogenesis attributed to the CPGs is created by the coupling of synergies and IMs, which are task specific. The system is also flexible as the same synergy can be employed by the neural pathways for both motions, and can explain variations in movement execution, as observed in neurophysiological studies [d'Avella et al., 2003, Severini et al., 2020, Zych et al., 2021].

This modular architecture is supported by the evidence of motor primitives and modularity of the CNS [Meunier et al., 2009]. The motor primitives are fundamental motor units codified at genetic level and can allow phylogenetic comparatives [Dominici et al., 2011]. Key parameters of the motor primitives (e.g., simplicity, modularity, recurrency, independence, or neural representation) are presented in the synergies. Modularity in the spinal cord has been proposed as spinal interneurons organized into functional motor modules that can be combined between them to display complex motor behaviours [Caggiano et al., 2016].

The MPL model assumes that human gait cycle is decomposable in five basic synergies [Ivanenko et al., 2004], where the activity of each synergy is triggered/inhibited by sensory afferents and the activity of some of the other synergies. Here we show that the MPL architecture 1) can achieve the STW transition, by changing the recruitment of the synergies; 2) only needs a unique signal to control the system while representing the principles of the legged mechanics; 3) presents synergies that can be shared between IMs; and 4) presents physiological gait and can transition between speeds of gait by modulating the controlling signal.

Here we present the results of optimizing the MPL model for the STW transition and for three different gait speeds (0.8, 1.2 and 1.6 ms^{-1}). In the simulations we show, the MPL model activates the IM for 'stand' at the beginning of the simulation. At the 5 second mark, the IM is switched to the 'walking' one. The model displays a human-like gait with kinematics and muscle activation patterns that are consistent with those presented by humans. Also, the tuning of a single control signal changes the parameters of the IM, allowing speed transitions ranging between 0.8 to 1.6 ms^{-1}.

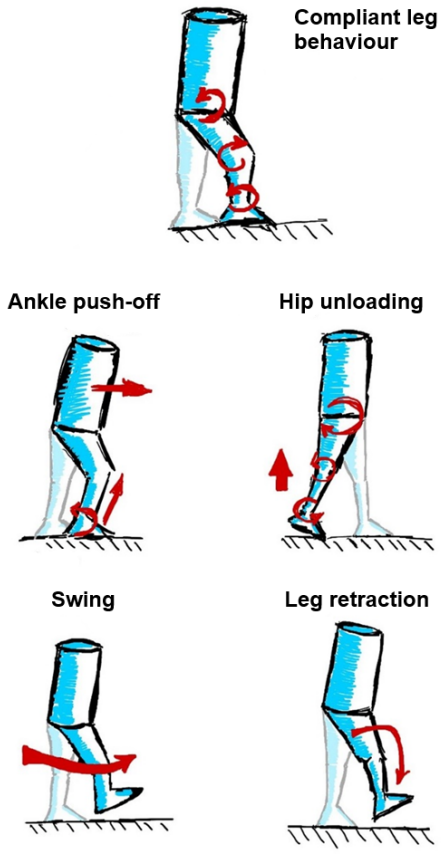

Figure 1: Principles of the legged mechanics. The figure presents the five principles of legged mechanics [Geyer and Herr, 2010], representative of the synergies implemented in the MPL controller

2 Methods

2.1 Musculoskeletal model

The musculoskeletal model was implemented on MATLAB R2022a following the proportions detailed in Geyer and Herr [2010], using the Simscape Multibody library. The model represents a human body of 1.80 m height and 80 kg weight. It has seven segments representing HAT (head-arms-torso), thighs, shanks, and feet. Feet are a composed structure where two segments are linked by a weld joint at their proximal ends. This union imitates the arch of the feet while their distal ends are the 'ball' and the 'heel'. The model has 6 degrees of freedom (DoF) as revolute joints connecting the segments (hips, knees, and ankles). Three additional DoFs were added to the model to define the movements of the biomechanical model with respect to the ground (longitudinal translation, anteroposterior translation, and pitch rotation). The muscle layer is composed of nine muscle tendon units (MTUs) implemented as hill-type muscle models as in Song and Geyer [2015]. The MTUs were gluteus, hip flexors, hamstrings, rectus femoris, vastus, biceps femoris short head, gastrocnemius, soleus, and tibialis anterior.

Finally, the contact geometry consists of four contact spheres of 4 cm radius placed at the balls and heels of each foot.

2.2 Hierarchical control layers

The controller consists of four layers organized in a hierarchical structure that represents different control processes of the CNS. From the higher to the lower position, these layers are the Control Layer, the Planner Layer, the Synergetic Layer, and the Premotor Area (Fig. 2).

The Control Layer is hypothetically placed in the midbrain. The layer has a unique component, the MLR, that sends a limited number of control signals (u_o) to the rest of the system to display different motor behaviours. The u_o can get

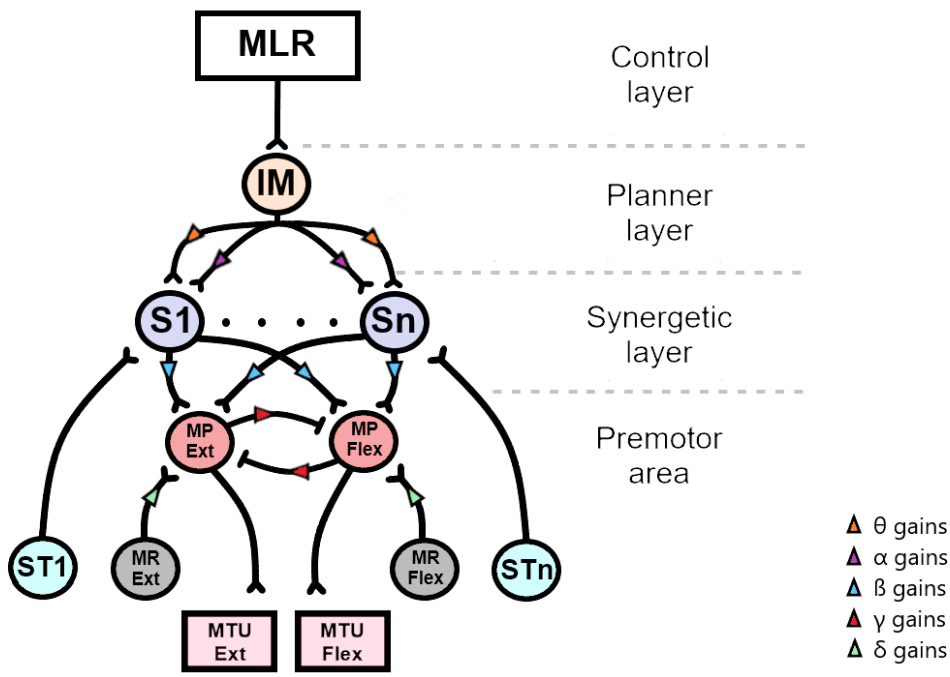

Figure 2: Scheme of the general approach of the MPL model. MLR: mesencephalic locomotor region, S: synergies, MP: motor pool (extensor and flexor), ST: sensory triggers, MR: monosynaptic reflexes, MTU: musculo-tendon units. Ext and Flex mean extensors and flexors for the joints (hips, knees, and ankles). Orange: α gains, purple: θ gains, blue: β gains, red: γ gains, green: δ gains.

different values depending on the movement and the IM to control. For quiet standing, where variants of the movement are not required, u_o is a discrete value that can be 0 or 1; inactive or active, respectively. In the case of modelling a dimension of a motor behaviour (e.g., speed of walking), u_o has continuous positive real values to generate a stronger, or faster, motor output.

The Planner Layer contains the IMs. The IMs control the expression of the synergies according to the u_o sent by the previous layer. The control exercised over the synergies is expressed by α gains, θ gains and interneurons. The α gains and the θ gains modulate the amplitude and the speed of burst of the synergies, respectively. The interneurons establish excitatory or inhibitory synapses between the synergies. These three elements ensure that the output of the neural pathway matches the expected behaviour (e.g., tonic activity for quiet standing, and rhythmogenesis for gait).

The Modular Layer encompasses the synergies. Synergies are independent between them, but the IM organizes a specific grouping in a neural pathway. Each synergy represents a simple motor response based on principles of human locomotion. A synergy is characterized by a sensory event that triggers a burst defined as:

$$S_i = \alpha(1 + cos(2\pi\eta\omega(u_o > 0) + \pi)) \tag{1}$$

where S_i is the output of the i-th synergy, η is a sensory modulation of the burst of activity, and ω is a modulation of speed of burst from another synergy. The parameter η is defined as:

$$\eta = \frac{\lambda_{Si}}{F_{Si} + \lambda_{Si}} \tag{2}$$

where λ_{Si} is a specific gain for the sensory afferent, F_{Si}, that modulates the i-th synergy. F_{Si} can be different from the sensory afferent that triggers the synergy or be absent. In the latter case, $F_{Si} = 0$, $\lambda_{Si} = 1$, $\eta = 1$. The parameter ω is defined as:

$$\omega = \frac{\pi}{\theta_{i+1} - \theta_i} \tag{3}$$

where θ_i and θ_{i+1} are the θ gains for the current and the next synergy in the movement cycle, respectively. In the model, each synergy is defined in a cycle that goes from 0 to 2π, whether it generates a rhythmogenesis or not. In the case where a single synergy is required for a neural pathway as in the case of quiet standing and the transition to walk, θ_{i+1} is the θ gain of a virtual synergy that defines the frequency of the bursts.

The last layer is the premotor area. The basic components of this layer are the motor pools, nuclei that integrate outputs from different sources and send an activation signal to the MTUs. Beside the synergies, each motor pool integrates the output of monosynaptic reflexes. The monosynaptic reflexes are specific for a motor pool, and do not stimulate muscles in synergy. The monosynaptic reflexes are represented by linear functions:

$$\kappa_k = \delta_k F_k \tag{4}$$

where κ_k is the k-th monosynaptic reflex for a motor pool, and δ_k is the synaptic weight of the k-th sensory afferent, F_k, to the motor pool. The motor pools are organized in pairs of antagonist muscles for hips, knees, and ankles. The activation output of the j-th motor pool is defined as:

$$y_i = \sum_{i=1}^{n} \beta_{ij} S_i + \sum_{k=1}^{m} \kappa_k - \gamma y' \tag{5}$$

where β_{ij} is the synaptic weight between the i-th synergy and the j-th motor pool, n is the number of motor pools in the system, and m is the number of monosynaptic reflexes connecting to that motor pool. The input y' is an inhibitory modulation from the antagonist motor pool, the synaptic weight of which is represented by γ. Each motor pool receives inputs from every synergy, but monosynaptic reflexes are specific for a motor pool. As β_{ij} can take positive or negative values, this structure allows synergies to inhibit the activity of monosynaptic reflexes.

2.3 Stand-To-Walk application

The architecture explained above is here applied to a specific scenario, that is a stand-to-walk (STW) transition. The model starts in a standing position, and when the MLR changes the IM, the body transitions to a steady gait that is maintained until the end of the simulation.

In this application, the MLR applies, at each instant of the simulation, one of three possible control signals: 'stand' ($u_{o,stand}$), 'gait' ($u_{o,gait}$), and an auxiliary signal to ease the 'transition' between stand and gait ($u_{o,trans}$).

As 'stand' is modeled as a static task, $u_{o,stand}$ has values 0 or 1, indicating whether the 'stand' IM is on or off. The control signal for transition, $u_{o,trans}$, is also set to 0 or 1, and is used to trigger a reaction to break the quiet standing. The speed of gait is modulated as a function of $u_{o,gait}$. Consequently, $u_{o,gait}$ can take different values starting from 0.

In the STW simulations we designed, the MLR changes the values of the u_o controls depending on the time of the simulation. At $t = 0$ s, $u_{o,stand} = 1$, $u_{o,trans} = 0$, and $u_{o,gait} = 0$, making 'stand' active. At $t = 5$ s, (t_{switch}), the MLR switches the control signals, $u_{o,stand} = 0$, and $u_{o,gait} > 0$, making 'gait' active. Previously, at pre-selected time before $t = 5$ s, $t_{switch} - t_{trans}$, $u_{o,trans}$ becomes 1 to switch again to 0 at t_{switch}. The 'transition' activity must be operative during a short period of time to execute the breaking movement. The start of this period is determined by t_{trans} and its value is calculated during the optimization process.

Each task (stand, transition, and gait) is overseen by one IM (IM_{stand}, IM_{trans} and IM_{gait}). IM_{stand} only activates one synergy and presents one α and one θ gain for that synergy, plus an additional θ for the virtual synergy regulating the final ω value as in equation (3). IM_{trans} also activates a single synergy and presents one α and one θ gain plus the virtual θ gain. IM_{gait} activates five synergies and presents five α and five θ gains.

The synergies represent the principles of legged mechanics [Geyer and Herr, 2010]. Each of them has associated sensory triggers and modulators (table 1), and are regulated by the gains of the IMs:

1) **Compliant leg behaviour.** It establishes a dynamic to resist gravity pull. This synergy is shared by both IMs, for 'stand', to keep legs extended and a quiet standing, and for 'gait', to resist gravity during heel strike, and confer double pendulum dynamics during the stance phase. The sensory trigger is the feet-ground contact of the leg to start stance (Ipsilateral leg load > 20 N). The synergy has a sensory modulator, the positive force

of the vastus muscle ($F_{S1} = VAS_{F^+}$). The gains associated with this synergy are $\alpha_{stand,1}$, $\alpha_{gait,1}$, $\theta_{stand,1}$, $\theta_{stand,2}$, $\theta_{gait,1}$, λ_{S1}, and β_{1j}.

2) **Ankle push-off.** The purpose of this synergy is the forward impulse of the body. It is triggered when the Centre-of-Mass (CoM) is stable inside the base of support ($CoM_x > heel_x$). The positive force of the soleus muscle ($F_{S2} = SOL_{F^+}$) acts as a sensory modulator. This synergy is only used in gait. The gains associated with this synergy are $\alpha_{gait,2}$, $\theta_{gait,2}$, λ_{S2}, and β_{2j}.

3) **Hip unloading.** In the late stance, this synergy assures that the stance leg unloads the weight of the body when the contralateral leg is ready for weight transfer. Thus, the sensory trigger is based on the contralateral leg load ($Load_{contra} < 20$ N). No sensory modulator is modelled for this synergy. This synergy is only used in gait. The gains associated with this synergy are $\alpha_{gait,3}$, $\theta_{gait,3}$, $\lambda_{S3} = 1$, β_{3j}.

4) **Swing.** The objective of this synergy is the forward impulse of the swing leg. The activity is triggered when the ipsilateral leg is free of the weight of the body ($Load_{ipsi} < 20$ N). No sensory modulator is modelled for this synergy. This synergy is only used in gait. The gains associated with this synergy are $\alpha_{gait,4}$, $\theta_{gait,4}$, $\lambda_{S4} = 1$, and β_{4j}.

5) **Leg retraction.** This synergy assures the landing of the swing leg. The activity is triggered when the heel of the swing leg reached the CoM ($Heel_x > CoM_x$). No sensory modulator is modelled for this synergy. This synergy is only used in gait. The gains associated with this synergy are $\alpha_{gait,5}$, $\theta_{gait,5}$, λ_{S5}, and β_{5j}.

6) **Transition.** Ad hoc synergy to ease the transition by breaking the quiet standing before t_{switch}. This synergy is not triggered by a sensory event but by the activation of the control signal ($u_{o,trans} > 0$), indicating a volitional change of movement. This synergy has a sensory modulator (F_{trans}) which is based on the forward leaning of the HAT. The gains associated with this synergy are $\alpha_{trans,6}$, $\theta_{trans,6}$, λ_{S6}, and β_{6j}. The synergy is only recruited by IM_{trans}.

Table 1: List of synergies and their corresponding function along the gait cycle, their corresponding sensory triggers and modulators, and the associated gains.

Synergy	Function	Trigger	Modulator (F_{Si})
1) Compliant leg behaviour	Resist gravity / keep quiet standing	Ipsilateral leg load > 20 N	$F_{S1} = VAS_{F^+}$
2) Ankle push-off	Forward impulse of the body	$CoM_x > heel_x$	$F_{S2} = SOL_{F^+}$
3) Hip unloading	Weight transference	$Load_{contra} < 20N$	-
4) Swing	Forward impulse of the swing leg	$Load_{ipsi} < 20N$	-
5) Leg retraction	Swing leg landing	$Heel_x > CoM_x$	-
6) Transition	Ease the STW transition	$u_{o,trans} > 0$	HAT_{Θ}

The coupling between the IM_{stand} and the compliant-leg-behaviour synergy creates the neural pathway to generate 'standing' activity, while the coupling between the IM_{gait} and the synergies 1-5 creates the neural pathway for 'gait'. The neural pathways include interneuron synapses to achieve the desired output of the synergies. Interneurons would establish connections that are normally inhibited by hypothetical inhibitory nuclei (In) (Fig. 3A). The IMs would inhibit these nuclei and thus elicit the activity of the interneurons, allowing the inhibition, or excitation, between synergies. For 'stand' an equivalent auto-excitatory synapsis is established for the burst of the compliant-leg-behaviour synergy to display the tonic activation (Fig. 3B). In terms of implementation, the tonic activation is achieved when the burst reaches its α value, and, thus, $y_1 = 2\alpha_{stand,1}$. This value is kept constant until the controlling signal is changed to $u_{o,gait}$. When the first synergy changes the gains to $\alpha_{gait,1}$ and $\theta_{gait,1}$, the burst dissipates. The 'transition' activity has the same behaviour, giving $y_6 = 2\alpha_{trans,6}$.

For 'gait', two equivalent inhibitory synapses are established between synergies according to its relative positions. A strong inhibitory synapsis is established from one synergy to the synergy two positions behind ($S_{i+2} \rightarrow S_i$). That means that $y_j = 0$ if $y_{i+2} > 0$. This mechanism avoids a synergy being still active when it is not needed anymore.

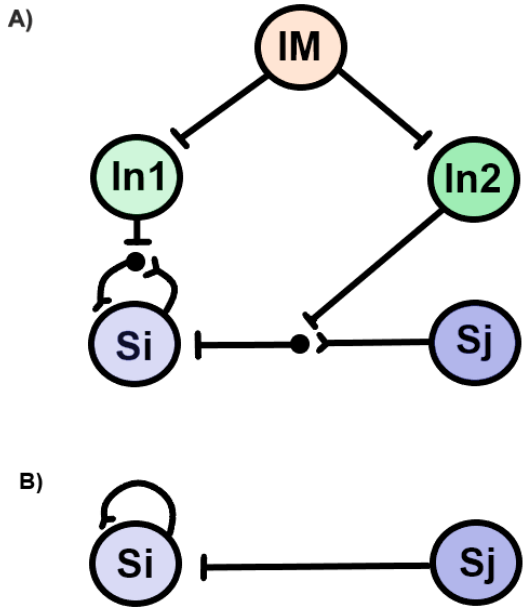

Figure 3: Inhibitory synapses between synergies. A) The synapses are suppressed by inhibitory nuclei (In1 and In2). The action of the IMs activates the interneurons. B) Equivalent synapses used for the implementation.

A second synapsis is established as a phase coupling [Strogatz, 2000]. Here, one synergy controls the rhythm of the previous synergy ($S_{i+1} \rightarrow S_i$). The phase coupling is defined as:

$$\Phi = -c \cdot sin(\phi_{i+1} + \phi_i + \pi) \tag{6}$$

where c is the strength of the coupling, and ϕ_i and ϕ_{i+1} are the phases of the first and the next synergy. Equation (1) then becomes:

$$S_i = \alpha(1 + cos(2\pi\eta\omega(u_o > 0) + \pi + \Phi)) \tag{7}$$

The synergies have a constant phase-delay of π, that is modulated by Φ. The relation of inhibitory interneurons for 'gait' is shown in Fig. 4.

An alternative formulation of (7) was devised for the first (compliant-leg-behaviour), the second (ankle-push-off), and the fifth (leg-retraction) synergies whose phase coupling was better explained by an amplitude factor:

$$S_i = \alpha(1 + cos(2\pi\eta\omega(u_o > 0) + \pi) - 10S_{i+1}) \tag{8}$$

At the level of the premotor area, the motor pools are constituted by the pairs of antagonists (flexors and extensors) muscles acting on each joint. In the case of the biarticular muscles, gastrocnemius, and hamstrings, they received the same input as soleus and gluteus, respectively, as their patterns during the gait cycle are similar. However, the activation input is scaled by a factor, S_{SOL} and S_{GLU}. The bi-articular rectus femoris is fed from the hip flexor motor pool and the extensor knee motor pools, with no scale factors, as its pattern presents similarities with vastus and hip flexors.

Additionally, monosynaptic reflexes feed the motor pools to modulate the output of both agonist and antagonist neural pathways. They are three linear reflexes to achieve stability in hips, knees, and ankles. The synaptic weights between the reflexes and the motor pools are modulated by δ gains. For hips:

$$F_{hip} = \begin{pmatrix} ((\phi_{hip} + \phi_{hip,o}(u_{o,gait} > 0)) & \dot{\phi}_{hip} \end{pmatrix} \begin{pmatrix} \delta_{q,ext} & \delta_{q,flex} \\ \delta_{w,ext} & \delta_{w,flex} \end{pmatrix} \tag{9}$$

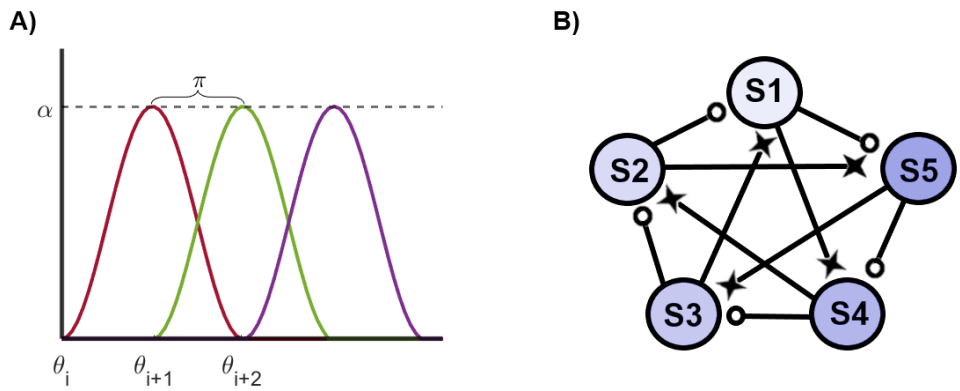

Figure 4: A) Representation of three successive synergies, red, green, and purple are i-th, i+1-th, and i+2-th synergies, respectively. B) Phase coupling (circle) and strong inhibitory (star) synapsis between the five synergies (anti-clockwise direction). For compliant-leg-behaviour, ankle-push-off and leg-retraction synergies the phase coupling is substituted by an amplitude inhibitory synapsis.

where F_{hip} is the sensory afferent for the antagonist pair, ϕ_{hip} is the angular position of the hip, $\phi_{hip,o}$ is the reference angular position (only active for 'gait'), $\dot{\phi}_{hip}$ is the angular velocity of the hip, $\delta_{q,ext}$ and $\delta_{q,flex}$ are the synaptic weights of the angular position to the extensor and the flexor motor pools, and $\delta_{w,ext}$ and $\delta_{w,flex}$ are the synaptic weights of the angular velocity to the extensor and the flexor motor pools, respectively, for the hip.

For the knee, the extensor motor pool is inhibited by 'pain', a measure of the knee joint extending beyond its soft limits. The sensory afferent, F_{knee}, is defined as:

$$F_{knee} = \delta_{knee} P_{knee} \tag{10}$$

where δ_{knee} is the synaptic weight for pain of the knee, P_{knee}.

The afferent for the motor pools of the ankle, F_{ankle}, is defined according to the relative contact force on the ball and the heel of the feet:

$$F_{ankle} = (\delta_{amkle,ext} \quad \delta_{akle,flex}) \frac{f_{ball}}{f_{heel} + f_{ball}} \tag{11}$$

where f_{ball} and f_{heel} are the contact force for the ball and the heel with the ground, and $\delta_{ankle,ext}$ and $\delta_{ankle,flex}$ are the synaptic weights for the extensor and flexor motor pool, respectively.

All the reflexes, including the monosynaptic and the synergies, present delays according to the position of the afferent source with respect to the body that can be classified as long, medium, and short delays. Finally, the inhibitory disynapsis between the pair of antagonists, represented by the γ gains (γ = $\{\gamma_{hip}, \gamma_{knee}, \gamma_{ank}\}$) are modified by the IM_{gait}, showing the ability of the IMs to modify the behaviour of the system beyond synergies:

$$\gamma' = \gamma + g(u_{o.gait} > 0) \tag{12}$$

where $g = \{g_{hip}, g_{knee}, g_{ank}\}$ are specific constants that modify the γ gains, and γ' are the transformed γ gains that are applied in equation (4). The schema of the model is presented in Fig. 5.

2.4 Speed transitions

STW supposes a transition from standing to walking, but also a continuous transition in walking speed until the goal speed (1.2 ms^{-1}) is achieved. IM_{gait} and $u_{o,gait}$ must then be adapted to show speed transitions inside the 5 s of walking simulation.

Here we link speed to the command u_o, by linking its value to the values of the $\alpha_{gait,i}$ and $\theta_{gait,i}$ gains following a linear function:

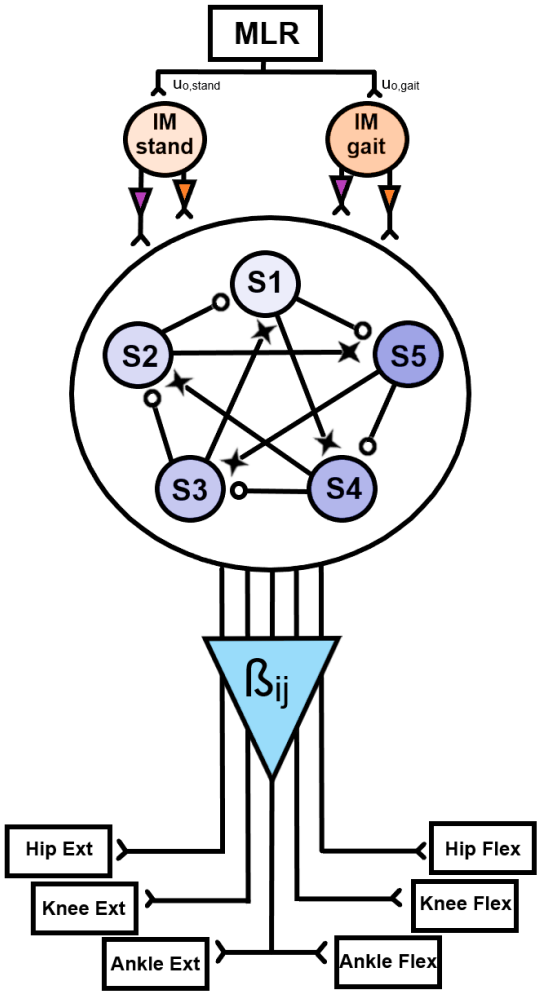

Figure 5: Specific application of the MPL model to the STW. Purple, orange, and green gains are α, θ, and β, respectively. MLR: mesencephalic locomotor region, u_o: controlling signal (stand, gait), IM: internal model (stand and gait), S_n: synergies, β_{ij}: beta gains for all the motor pools, rectangle boxes: motor pools for hips, knees, and ankles (extensor and flexor).

$$\alpha'_{gait,i} = \alpha_{gait,i} + \alpha_{gait,m,i} u_{gait,o} \tag{13}$$

$$\theta'_{gait,i} = \theta_{gait,i} + \theta_{gait,m,i} u_{gait,o} \tag{14}$$

where $\alpha_{gait,m,i}$ and $\theta_{gait,m,i}$ are synaptic weights that map the variations of u_o to specific new gains of the IM, $\alpha'_{gait,i}$ and $\theta'_{gait,i}$, respectively. Equations (1) and (2) are then modified.

The control signal, $u_{o,gait}$, is equal to 1 for the basic speed of 1.2 ms^{-1}. However, slower and faster gaits are reflected by lower and higher values of $u_{o,gait}$.

2.5 Optimization

The parameters of the controller (θ, and α gains of the three IMs, including the gains to map the speed transitions, the β, δ, γ, and g gains, the biarticular scale factors, and the variations of u_o to reach the different speeds, $u_{o,gait,up}$ and

$u_{o,gait,down}$) are selected through a multi-stage optimization process. The optimization process was implemented by using the Covariance Matrix Adaptation Evolution Strategy (CMA-ES) algorithm [Hansen, 2016]. To accomplish our aim of demonstrating that our model can switch from a stand task to a gait task, each task was optimized separately. The cost function for stance, J_{stand}, is:

$$J_{stand} = (t_{max} - t_{sim}) + E \tag{15}$$

where t_{max} is the maximum time of simulation set to 10 s, t_{sim} is the duration of the simulation in which the model does not fall, and E is the mass-specific energy consumption [Umberger et al., 2003]. E is defined as:

$$E = h_A + h_M + h_{SL} + w_{CE} \tag{16}$$

where h_A is the activation heat rate, h_M is the maintenance heat rate, and w_{CE} is the mechanical work rate of the contractile elements of the muscles. E is calculated over the duration of the simulation.

J_{stand} tries to maximize time without falling while minimizing energy consumption. The parameters to optimize are the delta gains and angular reference from (9) to (11), the λ_{S1} gain, all the β_{ij} gains, and the three γ gains of the motor pools, making a total of eighteen gains. The two θ gains of the IM_{stand} were hand-tuned to achieve a fast activation of the first synergy. The $\alpha_{stand,1}$ gain was set to 0.5, and $\theta_{stand,1}$ and $\theta_{stand,2}$ were set to 0 and 0.25.

Once 'stand' was complete, the parameters related to 'gait' were optimized. These parameters are the five $\alpha_{gait,i}$ gains and five $\theta_{gait,i}$ gains for the IM_{gait}, and the rest of the β gains of the system ($\beta_{ij} \backslash \beta_{1j}$). Also, t_{trans}, λ_{S2}, λ_{S6}, the scale factors, S_{SOL} and S_{HAM}, and the three g gains. In total, forty-eight parameters were optimized in this stage. The seventeen parameters from the stance optimization remained as constants. The gains $\alpha_{trans,6}$ and $\theta_{trans,6}$ were set to 0.5 and 0. Before applying the CMA-ES algorithm, the parameters were hand-tuned to achieve three steps. The cost function for gait (J_{gait}) is defined as:

$$J_{gait} = (t_{max} - t_{sim}) + 10\,|v_{tgt} - v_{sim}| + P + C \tag{17}$$

where t_{max} is set to 10 s, giving a 5 s for stand and gait, v_{tgt} is the objective speed of the simulation (at this stage, 1.2 ms^{-1}), v_{sim} is the average speed achieved during the simulation, P is pain and C is the metabolic cost of transport. C is defined as:

$$C = \frac{E \sum m_m}{m_{body} v_{sim}} \tag{18}$$

where m_m is the mass for each muscle and m_{body} is the whole mass of the body (80 kg).

For the optimization of speed transitions, we selected the parameters of a successful STW simulation. Once the simulation reaches a steady walking ($t = 6.5$ s), the $u_{o,gait}$ changes to some value above or below the default value for 1.2 ms^{-1} ($u_{o,gait} = 1$) for increasing or decreasing gait speed. These two values, $u_{o,gait,up}$ and $u_{o,gait,down}$, are optimized together with the twenty gains of the extension of the IM_{gait}, $\alpha_{gait,m,i}$ and $\theta_{gait,m,i}$. The cost function (J_{trans}) is defined as:

$$J_{trans} = 35\,|v_{tgt,last} - v_{sim,last}| + C + \frac{AP}{3} \tag{19}$$

where $v_{tgt,last}$ is the speed of the last gait cycle and can take the value of 0.8 or 1.6 ms^{-1}, $v_{sim,last}$ is the speed of the CoM_x in the last gait cycle, and AP is the deviations of the angular positions of the joints at heel strike respect to their mean. Two sets of $\alpha_{gait,m,i}$ and $\theta_{gait,m,i}$ were calculated for $u_{o,gait,up}$ and $u_{o,gait,down}$.

3 Results

3.1 Stand-To-Walk transition

The model transitions from stand to walking at t_{switch} ($t = 5$ s) according to the change of u_o and the IM (Fig. 6). The model maintains a stable quiet standing up to t_{switch}, even though it is slightly leaned backwards. At $t_{switch} - t_{trans}$ (approximately $t = 4.7$ s), IM_{trans} breaks the quiet standing, and the body leans forward. After t_{switch}, the model starts

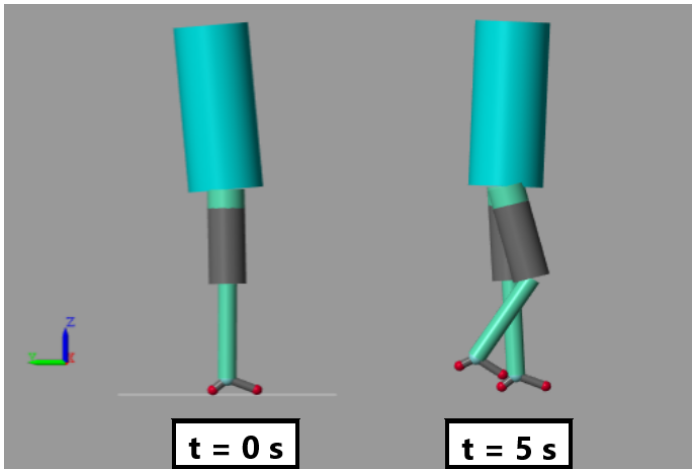

Figure 6: Representation of the 'stand' and 'walk' in simulations.

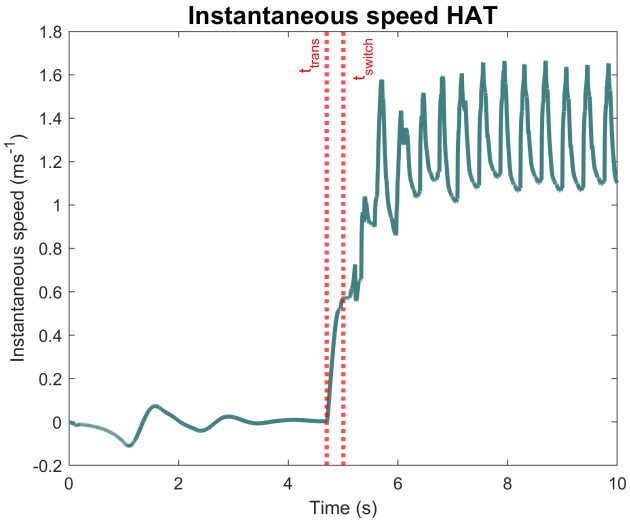

Figure 7: Instantaneous anterior/posterior speed of HAT shows the STW.

walking and reaches a steady walking at $t = 6.5$ s. The average walking speed is around 1.2 ms^{-1} and the average speed in the last step is 1.3 ms^{-1}. The instantaneous anterior/posterior speed of the HAT shows the transitions in Fig. 7.

Simulated data for the angular positions of hips, knees, and ankles during gait (5 s $< t <$ 10 s) were compared to experimental data [Fukuchi et al., 2018]. Fig. 8 shows the comparison of the simulated trajectory of the joints over the gait cycle (averaged from the last three steps of the walking phase) to the angular positions in humans. Results of the hips and knees are consistent to the experimental values. Ankles are consistent up to 50% of the gait cycle. For the second part of the cycle the simulated ankle presents plantar dorsiflexion. These observations are confirmed by a cross-correlation analysis. For hips and knees, the coefficients are above 0.8 (r_{hip} = 0.91, Δ_{hip} = 0; r_{knee} = 0.92, Δ_{knee} = 8). However, for ankle the coefficients are r_{ankle} = 0.42, Δ_{ankle} = -52.

In Fig. 9 muscle activation patterns are shown along the gait cycle and averaged from the last steps. Muscle activation patterns are consistent with those expected in humans [Zajac et al., 2003]. Biceps femoris and rectus femoris are the exception. Even though the second half of their patterns are close to physiological data, rectus femoris does not have activity in the first half of the gait cycle, while biceps femoris short head presents the expected peak, but it is shifted later than expected in the gait pattern.

Regarding the GRFs, left and right leg show the typical pattern of contact force [Zajac et al., 2003]. In Fig. 10 GRF is presented over the duration of walking, becoming steadily stable at $t = 6.5$ s. The two peaks of the human GRF are noticeable. However, the first peak is bigger than expected.

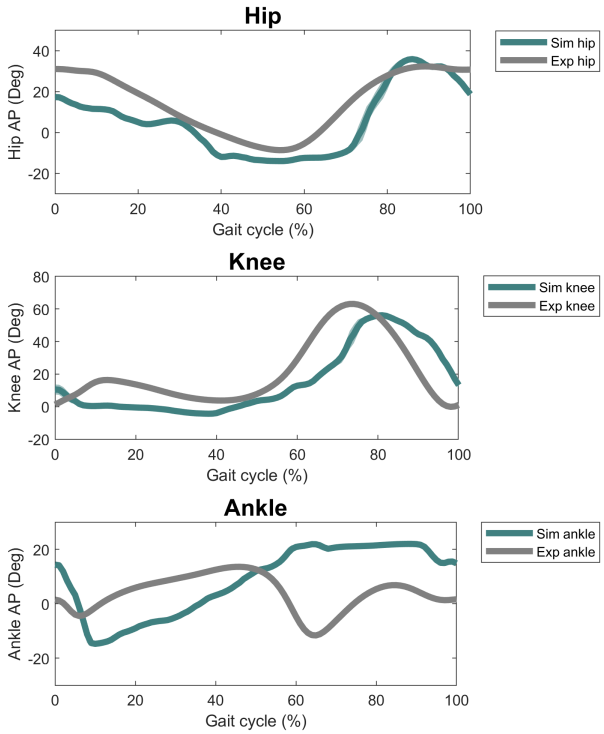

Figure 8: Experimental and simulated angular positions. Green: simulated data, grey: experimental data.

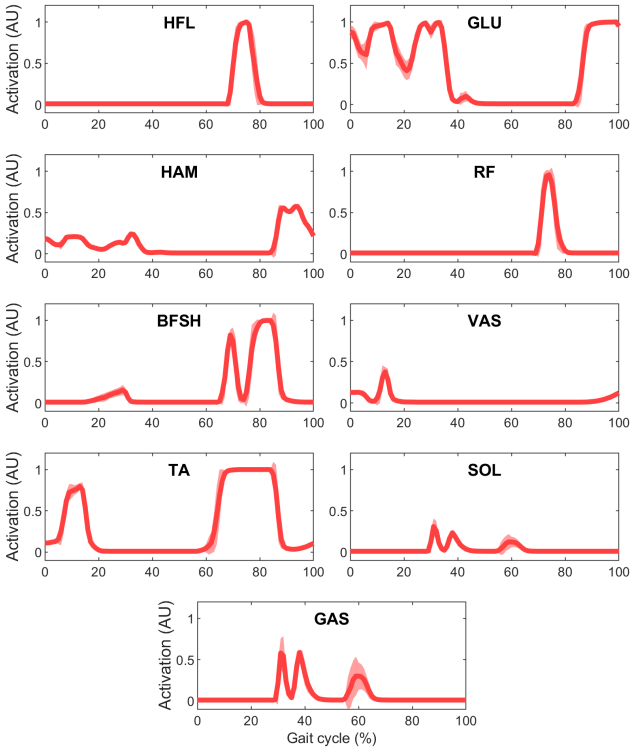

Figure 9: Muscle activation patterns for the left and right leg along the gait cycle.

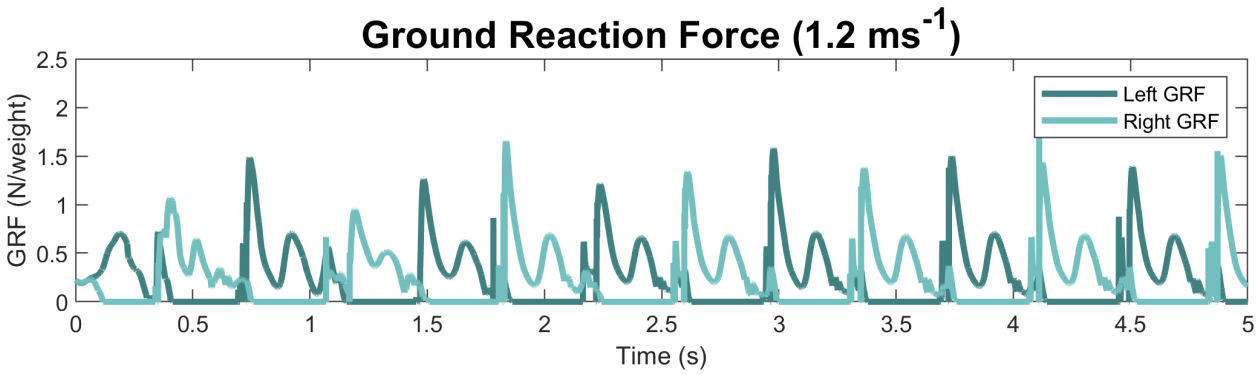

Figure 10: GRF for left and right foot along the duration of walking.

3.2 Speed transitions

Fig. 11 shows the speed transitions from 1.2 ms^{-1} to 0.8 and 1.6 ms^{-1}. At $t = 6.5$ s (t_{steady}), when the $u_{o,gait}$ switches to $u_{o,gait,down}$ or $u_{o,gait,up}$ and the new α and θ gains are applied, the instantaneous speed decreases or increases to achieve an average speed around 0.8 ms^{-1} and 1.6 ms^{-1}, respectively. In both cases a new steady gait is achieved. In the lower transition, the new steady walking is achieved approximately one second later than the transition to 1.6 ms^{-1}.

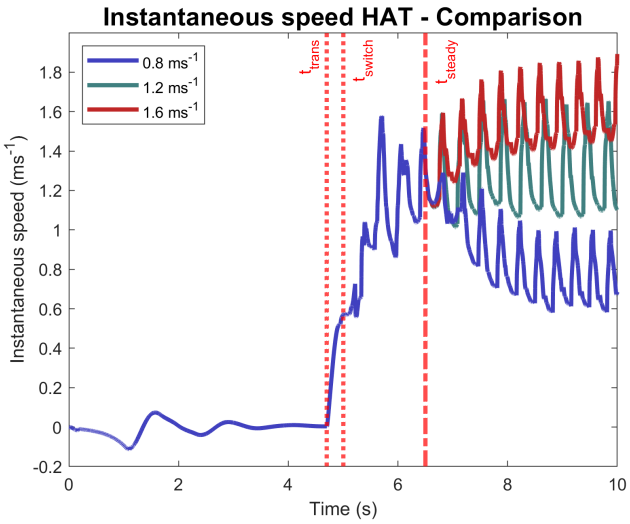

Figure 11: Instantaneous anterior/posterior speed of HAT along the STW for the default (1.2 m^{-1}), the lower (0.8 ms^{-1}) and the upper transitions (1.6 ms^{-1}) corresponding to the green, blue, and red lines, respectively.

The angular positions of the joints (average of the last three steps) in the lower and upper transitions are also consistent with experimental data of subjects walking at a slow and a fast pace [Fukuchi et al., 2018] (Fig. 12). The cross-correlation coefficients for hips and knees are high ($r_{hip,0.8} = 0.83$, $\Delta_{hip,0.8} = 0$; $r_{knee,0.8} = 0.87$, $\Delta_{knee,0.8} = 10$; $r_{hip,1.6} = 0.94$, $\Delta_{hip,1,6} = 1$; $r_{knee,1.6} = 0.87$, $\Delta_{knee,1.6} = 11$). However, in both cases the ankle also shows a bigger dorsiflexion in the second half of the gait cycle ($r_{ankle,0.8} = 0.45$, $\Delta_{ankle,0.8} = 36$; $r_{ankle,1.6} = 0.41$, $\Delta_{ankle,1.6} =$ -53).

The muscle activation patterns (average of the last three steps), as in the default speed (1.2 ms^{-1}), are consistent with the human patterns (Fig. 13). Again, the exceptions are the biceps femoris short head and the rectus femoris [Zajac et al., 2003].

GRF is similar to the sample of 1.2 ms^{-1} (Fig. 14) and to experimental samples [Zajac et al., 2003]. However, after achieving a steady gait, the difference from the first and the second peak is increased for the sample of 1.6 ms^{-1}, and attenuated for the sample of 0.8 ms^{-1}.

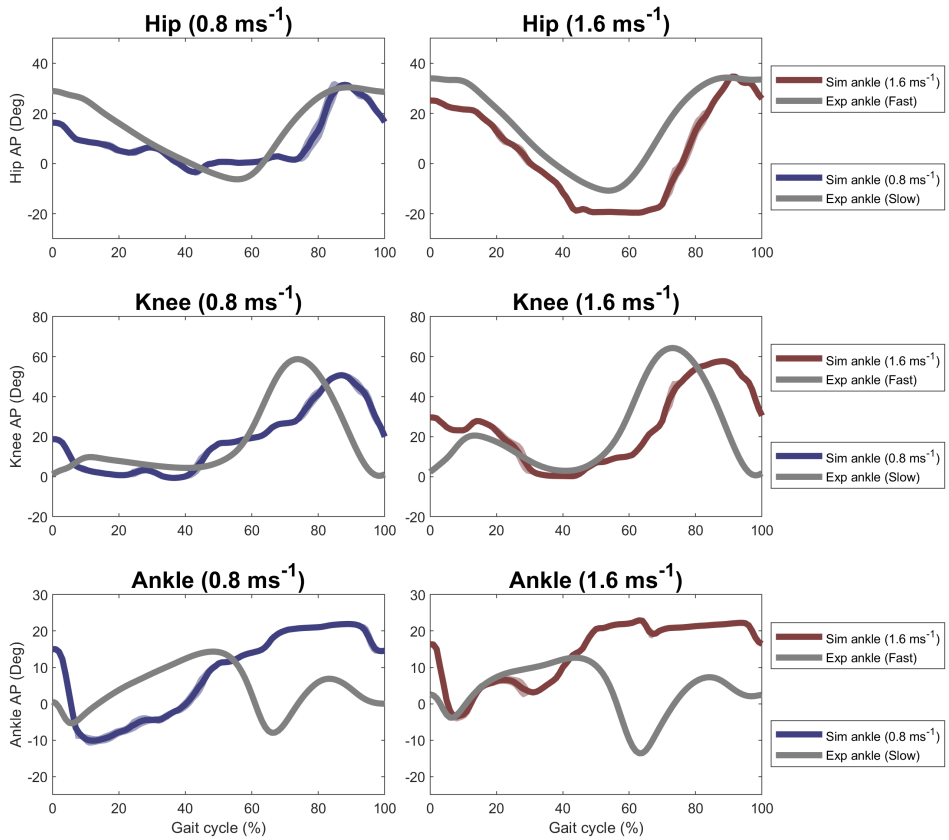

Figure 12: Experimental and simulated angular positions for the lower and the upper transitions.

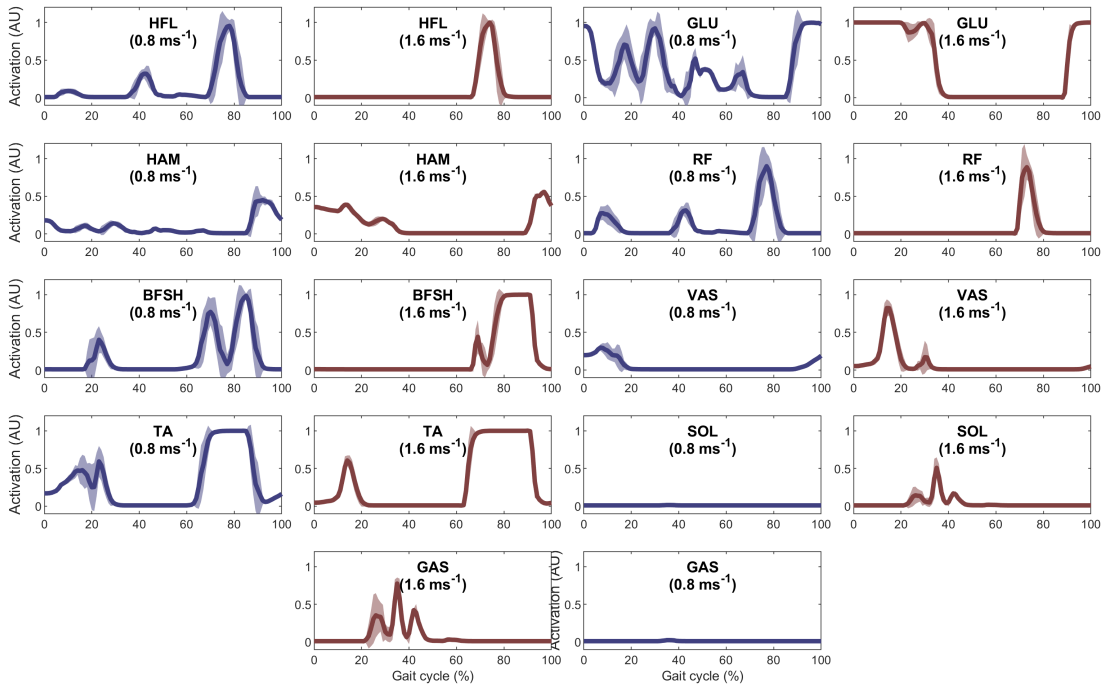

Figure 13: Muscle activation patterns for the left and right leg along the gait cycle for the lower and the upper transitions.

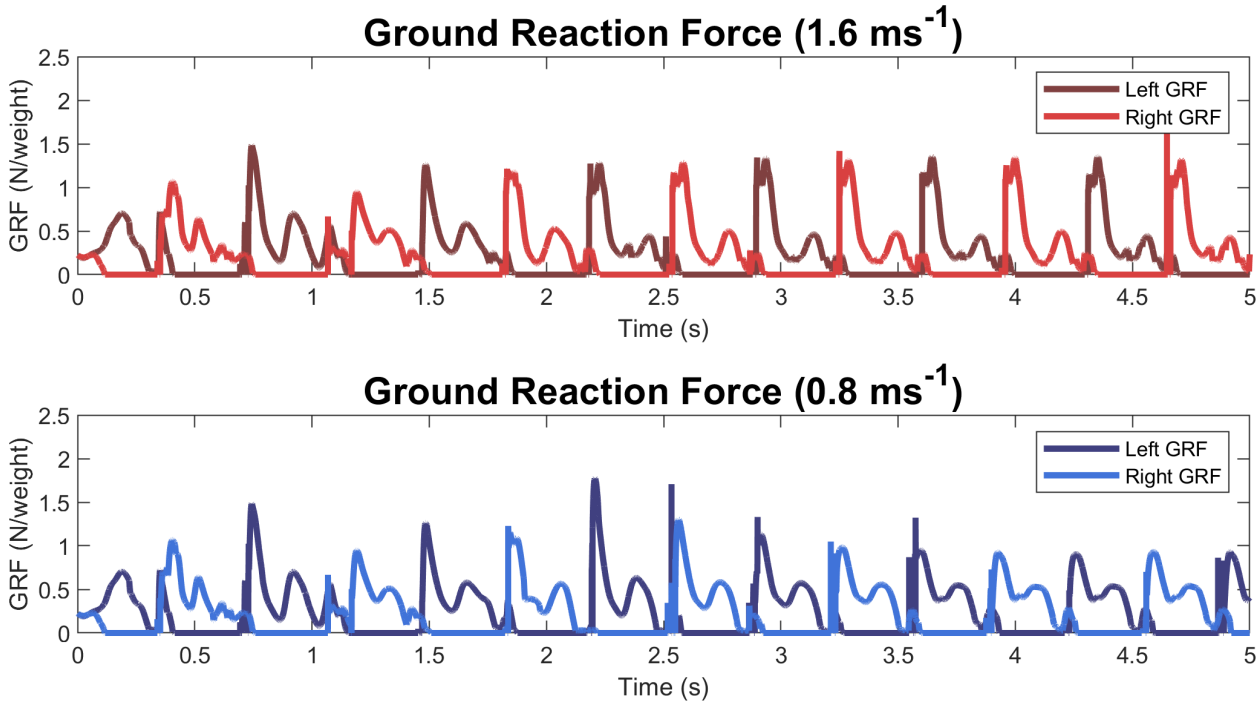

Figure 14: GRF for left and right foot along the duration of walking for the lower and the upper transitions.

4 Discussion

The MPL model is successful in replicating STW by the implementation of IMs and simple control signaling. The resulting kinematics and muscular activations are generally consistent with experimental data. The exceptions are the angular position of ankles and the muscle activation patterns of rectus femoris and biceps femoris during gait. In terms of control, the model is successful in modulating the speed of gait by tuning the controlling signal. The interplay of this signal and the parameters of the IM can adjust the rhythm of gait once stability is reached. The angular positions, muscle activation patterns and ground-reaction-forces are consistent through the change of speeds. We believe the MPL model was successful in achieving the objectives proposed for the STW transition. Stand and gait were mapped with a single control policy and the transition required the adjustment of a unique signal. As far we know, no previous models have been able to imitate a STW transition before. The MPL model introduces a new architecture that represents the multidimensional skill space with a simplified control.

PNM is typically challenged to simulate the physiological trajectory of the ankle. This could be because the dynamic stability of the CoM depends on the sensory responses to the CoP (Centre-of-Pressure) during the gait cycle [Dzeladini et al., 2014]. Thus, if the reflexes and the anatomy of the distal leg are improperly integrated with the rest of the system, the dynamics at this joint may be affected. For example, Song and Geyer [2015], Di Russo et al. [2023], and Ramadan et al. [2021] presented models with alterations at the ankles, the two last having discrepancies resembling those in the MPL model. Geyer and Herr [2010] presents ankle kinematics that fit better experimental data than our model, and Dzeladini et al. [2014] have also a better trajectory, especially if the controller is reflex-dependent. Schumacher et al. [2023] has shown results matching consistently with the kinematic data, but also presented abnormal trajectories for the ankle that were depending on the selection of the musculoskeletal model. This suggests that the coupling between the controller and the biomechanical characteristics of the model can alter the quality of the results, especially regarding the lack of anatomical detail in the foot.

Some previous reflex-based models such as Geyer and Herr [2010] or Song and Geyer [2015], produce results that are very close to human measurements. However, in order to perform the modulation of the gait speed, these models must optimise all the parameters of the controller. The MPL provides a simpler control. Once the model reached steady walking, it was possible to achieve transitions to slower and faster gaits, with variances from the original speed (1.2 ms^{-1}) of 0.4 ms^{-1}, achieved by adjusting the controlling signal. The organization of the different layers in a hierarchical structure, particularly the interplay of the IMs and the synergies, makes the MPL a versatile and flexible model.

In the case of CPG-based models, such as Taga et al. [1991], speed control was more efficient since the model could transition to running by employing also a unique controlling signal. However, the representation of CPGs, as a continuous oscillator in this case or sensory predictor in Dzeladini et al. [2014], is only marginally supported by physiological evidence on humans [Minassian et al., 2017]. However, the interaction between the IMs and the synergies permits the latter to be interpreted as components of a hypothetical CPG more similar to neuron-based proposals [Dzeladini et al., 2018]. Thus, the MPL model provides the potential to develop an architecture in which principles of biomechanics and neurophysiology can be represented while the control remains simple.

In our results, the ankle kinematics, the GRFs and the activations of the rectus femoris and biceps femoris are mostly consistent with their experimental counterparts, but the waveforms are altered in some points of the gait cycle. In the case of the ankle, its angular position is dorsiflexed in the second half of the cycle. This abnormality probably correlates with the asymmetry of the ground reaction force. In fact, the amplitude of the first peak of the GRF is bigger than the second one when they should be roughly at the same level. That means that the soleus and the gastrocnemius are not properly activated and do not generate the expected propulsion during the take-off phase. The absence of toe flexors can worsen these discrepancies, as ankle plantar flexion in the push-off must be supported by these muscles [Geyer and Herr, 2010]. Also, the stronger heel strike in the foot landing, that causes the first peak, can be due to the biomechanical coupling between stand and walk. While standing, the musculoskeletal model is slightly leaned backwards that must be adjusted to a forward inclination for walking. However, even though IM_{stand} was included to correct the inclination of the torso in the transition, the CoM could still be behind the right point of equilibrium and falling from a higher position during the foot landing.

In the case of the rectus femoris and the biceps femoris, during the first half of the cycle, their first peak of activity is absent or shifted later than expected in the gait cycle, respectively. These misplaced peaks may be caused by some incompatibility between the activity of the compliant-leg-behaviour synergy for 'stand' and 'walk'. It is possible that walking and standing do not share the compliant-leg-behaviour synergy. Alternatively, the shared synergy can be related to other aspects of 'stand' as reactive balance instead to create a tonic muscle activation [Allen et al., 2019]. In any case, the model demonstrates that it is possible to replicate different behaviours sharing the same synergies, however, it is possible that a more comprehensive vocabulary of synergies must be developed to correctly explain both quiet standing and gait.

The MPL model is the first attempt at a flexible, neurophysiologically plausible, controller which includes internal models. It is expected that the results of the simulations can be improved in future applications. In this work we used a relatively simple musculoskeletal model which may explain part of the discrepancy between simulated and experimental results [Geyer and Herr, 2010, Song and Geyer, 2015]. Although useful for evaluating a basic implementation of the MPL model, the musculoskeletal geometry and muscular implementation can be greatly improved. The simplicity of the model also impedes the comparison of the metabolic consumption, despite this measure is used in the cost functions.

A recent work has tested a reinforcement learning based controller on models of different complexity and using different physics environments for the tests [Schumacher et al., 2023]. The divergency in some metrics observed in that work when replicating gait suggests that the abnormalities presented in the MPL model may be caused by the interplay of the controller with the musculoskeletal model.

Although a natural next step for this work is to apply the current MPL controller to a more complex musculoskeletal model, there is also scope for further development of the controller. Here, as in similar works [Di Russo et al., 2023], we use sinusoidal bursts for the synergies, although more physiological activation profiles could be devised.

The dynamics of task transition can also be improved, by better characterizing the internal model IM_{trans} which regulates it. Also, synergies and monosynaptic reflexes may be reconfigured to display a better alternance of synergies [McCrea and Rybak, 2008] or a more complete and accurate motor response [Rossignol et al., 2006]. The implementation of these changes may allow to add simulations including perturbations or noisy sensory inputs to test the robustness of the architecture.

We also consider the potential of the MPL model to display features that were not presented here or in other works. As we see in the speed transitions, the alpha and theta gains of the IMs can modify the behaviour of the system. This implies that modifying these gains by a method that imitates a Hebbian learning, it could be possible to present motor learning [Krakauer et al., 2019]. As IMs are implemented locally (one set of IMs for each leg), this could allow the prediction of the dynamics observed on split-belt treadmill [Choi and Bastian, 2007], and robot-induced perturbations [Severini et al., 2020] experiments. Also, altering synergies in more developed versions of the MPL model, pathological conditions, such as stroke, can be replicated, and try to simulate compensatory mechanisms through modification θ and α gains of the IMs.

The future achievement of these objectives may allow for the MPL model to be used to test neurophysiological processes that cannot be assessed in conventional experiments and other neuromuscular models.

References

Friedl De Groote and Antoine Falisse. Perspective on musculoskeletal modelling and predictive simulations of human movement to assess the neuromechanics of gait. *Proceedings of the Royal Society B*, 288(1946):20202432, 2021.

Friedl De Groote, Allison L Kinney, Anil V Rao, and Benjamin J Fregly. Evaluation of direct collocation optimal control problem formulations for solving the muscle redundancy problem. *Annals of biomedical engineering*, 44: 2922–2936, 2016.

Antoine Falisse, Gil Serrancolí, Christopher L Dembia, Joris Gillis, and Friedl De Groote. Algorithmic differentiation improves the computational efficiency of opensim-based trajectory optimization of human movement. *PLoS One*, 14 (10):e0217730, 2019.

Andrea Di Russo, Dimitar Stanev, Anushree Sabnis, Simon M Danner, Jessica Ausborn, Stephane Armand, and Auke Ijspeert. Investigating the roles of reflexes and central pattern generators in the control and modulation of human locomotion using a physiologically plausible neuromechanical model. *bioRxiv*, pages 2023–01, 2023.

Gentaro Taga, Yoko Yamaguchi, and Hiroshi Shimizu. Self-organized control of bipedal locomotion by neural oscillators in unpredictable environment. *Biological cybernetics*, 65(3):147–159, 1991.

Hartmut Geyer and Hugh Herr. A muscle-reflex model that encodes principles of legged mechanics produces human walking dynamics and muscle activities. *IEEE Transactions on neural systems and rehabilitation engineering*, 18(3): 263–273, 2010.

David Muñoz, Cristiano De Marchis, Leonardo Gizzi, and Giacomo Severini. Predictive simulation of sit-to-stand based on reflexive-controllers. *Plos one*, 17(12):e0279300, 2022.

Charles Capaday. The special nature of human walking and its neural control. *TRENDS in Neurosciences*, 25(7): 370–376, 2002.

Rachid Ramadan, Hartmut Geyer, John J Jeka, Gregor Schöner, and Hendrik Reimann. A neuromuscular model of human locomotion combines spinal. 2021.

Daniel M Wolpert, R Chris Miall, and Mitsuo Kawato. Internal models in the cerebellum. *Trends in cognitive sciences*, 2(9):338–347, 1998.

Mitsuo Kawato. Internal models for motor control and trajectory planning. *Current opinion in neurobiology*, 9(6): 718–727, 1999.

Vittorio Caggiano, Vincent CK Cheung, and Emilio Bizzi. An optogenetic demonstration of motor modularity in the mammalian spinal cord. *Scientific reports*, 6(1):35185, 2016.

Yuri P Ivanenko, Richard E Poppele, and Francesco Lacquaniti. Motor control programs and walking. *The Neuroscientist*, 12(4):339–348, 2006.

Ariel J Levine, Christopher A Hinckley, Kathryn L Hilde, Shawn P Driscoll, Tiffany H Poon, Jessica M Montgomery, and Samuel L Pfaff. Identification of a cellular node for motor control pathways. *Nature neuroscience*, 17(4): 586–593, 2014.

Didier Le Ray, Laurent Juvin, Dimitri Ryczko, and Réjean Dubuc. Supraspinal control of locomotion: the mesencephalic locomotor region. *Progress in brain research*, 188:51–70, 2011.

Andrea d'Avella, Philippe Saltiel, and Emilio Bizzi. Combinations of muscle synergies in the construction of a natural motor behavior. *Nature neuroscience*, 6(3):300–308, 2003.

Giacomo Severini, Alexander Koenig, Catherine Adans-Dester, Iahn Cajigas, Vincent CK Cheung, and Paolo Bonato. Robot-driven locomotor perturbations reveal synergy-mediated, context-dependent feedforward and feedback mechanisms of adaptation. *Scientific reports*, 10(1):5104, 2020.

Magdalena Zych, Annalisa Cannariato, Paolo Bonato, and Giacomo Severini. Forward and backward walking share the same motor modules and locomotor adaptation strategies. *Heliyon*, 7(8), 2021.

David Meunier, Renaud Lambiotte, Alex Fornito, Karen Ersche, and Edward T Bullmore. Hierarchical modularity in human brain functional networks. *Frontiers in neuroinformatics*, 3:571, 2009.

Nadia Dominici, Yuri P Ivanenko, Germana Cappellini, Andrea d'Avella, Vito Mondì, Marika Cicchese, Adele Fabiano, Tiziana Silei, Ambrogio Di Paolo, Carlo Giannini, et al. Locomotor primitives in newborn babies and their development. *Science*, 334(6058):997–999, 2011.

Yuri P Ivanenko, Richard E Poppele, and Francesco Lacquaniti. Five basic muscle activation patterns account for muscle activity during human locomotion. *The Journal of physiology*, 556(1):267–282, 2004.

Seungmoon Song and Hartmut Geyer. A neural circuitry that emphasizes spinal feedback generates diverse behaviours of human locomotion. *The Journal of physiology*, 593(16):3493–3511, 2015.

Steven H Strogatz. From kuramoto to crawford: exploring the onset of synchronization in populations of coupled oscillators. *Physica D: Nonlinear Phenomena*, 143(1-4):1–20, 2000.

Nikolaus Hansen. The cma evolution strategy: A tutorial. *arXiv preprint arXiv:1604.00772*, 2016.

Brian R Umberger, Karin GM Gerritsen, and Philip E Martin. A model of human muscle energy expenditure. *Computer methods in biomechanics and biomedical engineering*, 6(2):99–111, 2003.

Claudiane A Fukuchi, Reginaldo K Fukuchi, and Marcos Duarte. A public dataset of overground and treadmill walking kinematics and kinetics in healthy individuals. *PeerJ*, 6:e4640, 2018.

Felix E Zajac, Richard R Neptune, and Steven A Kautz. Biomechanics and muscle coordination of human walking: part ii: lessons from dynamical simulations and clinical implications. *Gait & posture*, 17(1):1–17, 2003.

Florin Dzeladini, Jesse Van Den Kieboom, and Auke Ijspeert. The contribution of a central pattern generator in a reflex-based neuromuscular model. *Frontiers in human neuroscience*, 8:371, 2014.

Pierre Schumacher, Thomas Geijtenbeek, Vittorio Caggiano, Vikash Kumar, Syn Schmitt, Georg Martius, and Daniel FB Haeufle. Natural and robust walking using reinforcement learning without demonstrations in high-dimensional musculoskeletal models. *arXiv preprint arXiv:2309.02976*, 2023.

Karen Minassian, Ursula S Hofstoetter, Florin Dzeladini, Pierre A Guertin, and Auke Ijspeert. The human central pattern generator for locomotion: Does it exist and contribute to walking? *The Neuroscientist*, 23(6):649–663, 2017.

Florin Dzeladini, Nadine Ait-Bouziad, and Auke Ijspeert. Cpg-based control of humanoid robot locomotion. *Humanoid Robotics: A Reference*, pages 1–35, 2018.

Jessica L Allen, Trisha M Kesar, and Lena H Ting. Motor module generalization across balance and walking is impaired after stroke. *Journal of Neurophysiology*, 122(1):277–289, 2019.

David A McCrea and Ilya A Rybak. Organization of mammalian locomotor rhythm and pattern generation. *Brain research reviews*, 57(1):134–146, 2008.

Serge Rossignol, Réjean Dubuc, and Jean-Pierre Gossard. Dynamic sensorimotor interactions in locomotion. *Physiological reviews*, 86(1):89–154, 2006.

John W Krakauer, Alkis M Hadjiosif, Jing Xu, Aaron L Wong, and Adrian M Haith. Motor learning. *Compr Physiol*, 9 (2):613–663, 2019.

Julia T Choi and Amy J Bastian. Adaptation reveals independent control networks for human walking. *Nature neuroscience*, 10(8):1055–1062, 2007.